Sustainable Food Technology

ROYAL SOCIETY OF CHEMISTRY

PAPER

View Article Online
View Journal

Cite this: DOI: 10.1039/d5fb00470e

Photodynamic regulation of potato greening: sodium copper chlorophyllin-functionalized alginate/sanxan nanocomposite films with spectral-selective barrier properties

Erihemu, * Chuchu Zhang, Hongze Lv, Ke Shi, Jing Wang, Fan Yang, Yi Wu, Hui Ma, Pengfei Zhang and Wenliang Qi

An innovative sodium alginate/sanxan (SA/SAN) composite film incorporating sodium copper chlorophyllin (SCC) was used to control postharvest potato tuber greening. Comprehensive investigations were conducted on the stability of SCC and the composite film's physicochemical properties and anti-greening efficacy. Results demonstrated that SCC exhibited strong absorption at 402 nm and excellent light, thermal, and pH stability and enhanced the mechanical strength of the SA/SAN films (18% increase in tensile strength at 0.4% SCC) while reducing moisture content and improving barrier properties (11% lower water vapor transmission rate at 2% SCC). The SA/SAN/SCC composite films showed substantial UV and blue-light blocking (transmittance of <20% at 200–315 nm and <40% at 400–450 nm), which are crucial for suppressing total chlorophyll (TC) synthesis. Notably, potato tubers coated with SA/SAN/SCC (2%) showed considerably reduced greening, 25.82% decrease in TC content after 72 h and sustained inhibition after over 60 days of storage. X-ray diffraction and thermogravimetric analyses confirmed enhanced intermolecular interactions and thermal stability in the SCC-incorporated films. These findings establish an effective and eco-friendly strategy for preventing potato tuber greening, offering foundational insights for the development of advanced food preservation materials.

Received 10th August 2025
Accepted 1st November 2025

DOI: 10.1039/d5fb00470e

rsc.li/susfoodtech

Sustainability spotlight

This study demonstrates a sustainable approach to controlling postharvest potato greening by developing an SA/SAN/SCC composite film that combines biodegradable polysaccharides (sodium alginate/sanxan) with food-grade sodium copper chlorophyllin (SCC). The film effectively blocks UV (200–315 nm, <20% transmittance) and chlorophyll-inducing blue light (400–450 nm, <40% transmittance), reducing greening by 25.82% within 72 h and maintaining inhibition over 60 days of storage. With optimized thickness (0.047–0.048 mm) and SCC incorporation (0.4–2.0%), the film enhances tensile strength (18% increase) and barrier properties (11% lower WVTR) while minimizing material usage. The solution avoids synthetic plastics, improves food preservation efficiency, and reduces postharvest losses, aligning with sustainable packaging and food waste reduction goals.

1. Introduction

Potatoes are ideal energy-rich food sources because of their high nutritional value and versatility in processing applications. After harvesting, they can be stored for several months under appropriate conditions, rendering them an ideal energy-rich food source.[1] However, during the postharvest supply chain processes (including harvesting, transportation, storage, and marketing), potatoes are inevitably exposed to light, which not only induces tuber skin greening but also triggers the synthesis of toxic glycoalkaloids and poses potential food safety risks. Consequently, in practical production, greening is often used as a key indicator for assessing toxic alkaloid accumulation.[2] Greened potatoes exhibit not only green discoloration and bitter taste but also decline in sensory quality and commercial value. These effects contribute to substantial economic losses, severely constraining the development of the potato industry.[3] Therefore, the effective prevention and control of potato greening is of considerable practical importance for reducing economic losses in the industry and mitigating health risks associated with toxic alkaloids.

The biological basis of potato tuber greening lies in the abnormal light-induced accumulation of chlorophyll (Chl) in cells.[4] Upon exposure to light stimuli, plastid membranes in potato cells, which are rich in amyloplasts, undergo substantial structural reorganization, during which inner membrane folding leads to thylakoid formation. After prolonged illumination, the number of thylakoids increases exponentially, and the grana lamellae organize into well-ordered stacks. These

Department of Food Science, Shanxi Normal University, Taiyuan, Shanxi, 030006, China. E-mail: erihemu_sxnu_ed@126.com

structural changes ultimately facilitate the full conversion of amyloplasts into functional chloroplasts. Plastid transformation process occurs concomitantly with the progressive expression of photosystem II-related proteins, establishing the structural framework necessary for Chl biosynthesis and accumulation.[5] However, potatoes exhibit varying sensitivity to specific wavelengths within the visible light spectrum. Spectral analyses have demonstrated that potato tubers display characteristic absorption spectra with three distinct peaks corresponding to blue, yellow, and red wavelengths while showing minimal absorption in the green spectral region.[6] Consequently, the targeted modulation of light absorption spectra is a viable strategy for suppressing Chl biosynthesis and accumulation in potato tubers during storage or transport through the selective filtering or attenuation of specific wavelength ranges.

Biodegradable films and coatings have emerged as pivotal solutions in food preservation technology and distinguished by their unique material attributes and multifunctional benefits.[7] These advanced materials not only exhibit exceptional properties, including biodegradability, renewability, cost-effectiveness, material abundance, nontoxicity, and biocompatibility, but also considerably enhance postharvest preservation efficacy in fruits and veges through synergistic mechanisms.[8] Polysaccharide-based edible coatings, especially sodium alginate (SA) formulations, can markedly improve multiple food quality attributes during storage.[9–12] As a linear polysaccharide copolymer with polyanionic characteristics, SA offers several benefits, including excellent water solubility, biodegradability, and inherent biocompatibility.[13] Its hydrophilic nature, coupled with its remarkable bio-adhesive properties and cost-effectiveness, renders it particularly suitable for various coating formulations.[14] Furthermore, the nontoxic nature of SA has prompted extensive investigation into its postharvest quality control, particularly for edible coatings on fruits and vegetables.[15–17] Moreover, Sanxan (SAN), which is a novel microbial exopolysaccharide, exhibits distinctive physicochemical properties, including an anionic heteropolysaccharide structure, exceptional low-concentration viscosity, outstanding film-forming capacity, and remarkable biocompatibility. Notably, its thermoreversible gelation behavior and pH-resistant characteristics have contributed to its broad application across agricultural and food sectors.[18] Mechanistically, SAN has been demonstrated to considerably enhance the water-holding capacities and mechanical properties of composite films.[19]

Sodium copper chlorophyllin (SCC), a semi-synthetic water-soluble Chl derivative, has been approved by the FDA as a food coloring agent (E141) with recognized safety and is widely used in pharmaceutical, cosmetic, and food industries.[20] Additionally, SCC exhibits significantly superior stability to natural Chl in terms of light, heat, and pH resistance, ensuring the long-term performance of coatings during storage.[21] More importantly, its molecular structure confers unique optical properties, exhibiting two characteristic absorption peaks at 405 nm and 630 nm in the visible spectrum.[22] This spectral range closely matches the blue light band (400–500 nm) that strongly induces Chl synthesis and greening in potatoes.[6] Although natural pigments like anthocyanins and curcumin can shield certain wavelengths, SCC combines water solubility, regulatory compliance, and precise blue light blocking capabilities, making it an ideal material for developing targeted anti-green coloration light-shielding coatings for potatoes. To the best of our knowledge, no prior studies have investigated whether SCC-enriched edible SA/SAN coatings can affect or inhibit potato tuber greening during storage. Thus, the objectives of this research are to evaluate the combined effect of SCC on the properties of SA/SAN films and to investigate the efficacy of SA/SAN/SCC solutions in inhibiting potato tuber greening during storage.

2. Materials and methods

2.1. Materials

Potato tubers (Jinshu 16) were cultivated in Lanxian County, Lvliang City, Shanxi Province (38.2770° N, 111.6170° E), and harvested in September 2023. After harvest, tubers were cured for 14 days in a ventilated room maintained at 15–18 °C and 85–90% relative humidity. Before experiments, disease-free tubers of uniform size (about 200 g) without mechanical damage were selected and stored at 4 °C and 85–90% relative humidity until use. All the chemicals used were of analytical grade and obtained from the following suppliers: SA (CAS No. 9005-38-3, M_w = 86 537 g mol^{-1}, viscosity 200 ± 20 mPa s, G/M ratio of 1, drying loss rate ≤15%, purity >99%), sodium hydroxide (NaOH, 96%), and potassium hydroxide (KOH, 85%) were purchased from Tianjin Yongda Chemical Reagent Co., Ltd (Tianjin, China); food-grade SAN (the fermentation product of *Sphingomonas sanxanigenens*, M_w: 408 kDa, M_n: 382 kDa, dispersity ($Đ$): 1.07) was acquired from Hebei Xinhe Biochemical Co., Ltd (Hebei, China); SCC (CAS No. 11006-34-1, M_w: 724.15 Da), glycerol, and calcium chloride ($CaCl_2$, 96%) were sourced from Shanghai Mclinn Biochemical Technology Co., Ltd (Shanghai, China).

2.2. Stability analysis of SCC

2.2.1. Spectroscopic absorption characteristics of SCC. The stability analytical procedure outlined by Li *et al.*[22] was adopted with methodological modifications. All the solutions were prepared using ultrapure water under controlled ambient conditions (25 °C). SCC was precisely weighed (0.2 g) and quantitatively transferred to a volumetric flask. The powder was completely dissolved in 100 mL of distilled water under magnetic stirring (800 rpm, 15 min) to yield a homogeneous 2 mg mL^{-1} stock solution. Stock solution (2.5 mL) was transferred to a 500 mL volumetric flask with a calibrated micropipette, and the solution was brought to a final volume with distilled water and mixed to yield a 0.1 mg mL^{-1} working standard. Absorption spectra were acquired using a UV–Vis spectrophotometer (L5S, Shanghai Analytical Instrument Co., Ltd, Shanghai, China) within a range of 350–700 nm.

2.2.2. Effect of illumination duration on the stability of SCC. The photostability of SCC was evaluated using the experimental procedure outlined by Yao *et al.* with modifications.[23]

Two aliquots (20 mL each) of 0.1 mg mL^{-1} SCC solution were transferred to conical flasks (50 mL). The samples were divided and placed in two distinct controlled environments: maintained in light-proof chambers and subjected to continuous illumination (3000 lux, 25 °C). Absorbance measurements ($\lambda = 402$ nm) were conducted at predetermined intervals (0, 2, 4, 6, and 8 days) with a calibrated UV–Vis spectrophotometer (L5S, Shanghai Analytical Instrument Co., Ltd, Shanghai, China).

2.2.3. Effect of temperature on the stability of SCC. The experiment was conducted using the procedures outlined by Zhong *et al.* with optimizations.[24] Five aliquots (20 mL each) of 0.1 mg mL^{-1} SCC solution were dispensed into separate glass test tubes (50 mL). The samples were incubated in water baths at 20 °C, 40 °C, 60 °C, 80 °C, and 100 °C for 20 min, followed by immediate ice-bath quenching (4 °C, 5 min). Absorbance was quantified at 402 nm (L5S, Shanghai Analytical Instrument Co., Ltd, Shanghai, China) after temperature equilibration to 25 °C. Each measurement was performed in triplicate.

2.2.4. Effect of pH on the stability of SCC. The absorbance of SCC at different pH values was measured according to the method described by Zhang *et al.* with minor modifications.[25] Six test tubes were each filled with 20 mL of 0.1 mg mL^{-1} SCC solution. The pH of the solutions was then adjusted to 2, 4, 6, 8, 10, and 12 with 0.1% NaOH and 0.1% HCl. Subsequently, the samples were stored at 4 °C for 30 min before their absorbance at 402 nm was measured.

2.3. Preparation of composite films

SA/SAN/SCC composite films were prepared using the casting method. First, based on the results of pre-experiments, 0.5 g of SA and 0.1 g of $CaCl_2$ (as a cross-linking agent) were dissolved in 100 mL of distilled water and stirred at 1000 rpm for 10 min to ensure complete dissolution. Subsequently, 0.5 g of SAN was added and stirred continuously for 30 min at 45 °C to obtain a homogeneous SA/SAN mixture. Then, SCC solutions with different concentrations (0.4%, 1.2%, 2%, 2.8%, and 3.6%, w/v) and 0.4 g of glycerol were added to the mixture sequentially, and stirring was continued for 30 min to ensure sufficient mixing. The resulting mixture was then allowed to stand undisturbed for 24 h to eliminate air bubbles. The film was formed by casting, and 30 mL of the defoamed film solution was evenly poured in a 10 cm × 10 cm plastic Petri dish and then dried in an oven at 35 °C for 24 h. Finally, the composite membrane was placed in an incubator with constant temperature (25 ± 2 °C) and humidity (50% ± 5% relative humidity) for 48 h (Fig. 1). The composite membrane was then stabilized for subsequent characterization and analysis.

2.4. Characterization of films

2.4.1. Visual appearance and chromatic aberration. The films were cut into uniform squares measuring 4 cm × 4 cm, and the visual appearance of the films was recorded through photography. The chromatic aberration of the films was measured using the method outlined by Dong *et al.*[26] The a^* values of the composite films were determined using a CR-400 colorimeter (Guangdong Sanenshi Intelligent Technology Co., Ltd, Shenzhen, China). Five replicate measurements were performed per film, and the average values were calculated.

2.4.2. Thickness. Each film was laid flat on a glass square dish, and measurements were obtained at the center and four corners with a digital thickness gauge with an accuracy of 0.001 mm. The final thickness value was calculated as the average of five replicate measurements at each position.

2.4.3. Mechanical properties. Tensile strength (TS, MPa) and elongation at break (EAB, %) were determined using the method outlined by Tang *et al.* with some modifications.[27] The films were cut into rectangles measuring 70 mm × 10 mm and fixed in the fixture of a TA.XTplus texture analyzer (Stable Micro Systems, Godalming, UK). The distance between the fixture brackets (called initial spacing) was 40 mm, the trigger force for the test was 0.05 N, and the tensile speed was 0.2 mm s^{-1}. TS and EAB were calculated using eqn (1) and (2).

$$\mathrm{TS}\ (\mathrm{MPa}) = \frac{F_\mathrm{M}}{A \times B} \quad (1)$$

where F_M (N) is the maximum force at break, A (mm) is the width of the film strips, and B (mm) is the length of the film strips.

$$\mathrm{EAB}\ (\%) = \frac{\Delta L}{L_0} \times 100\% \quad (2)$$

where ΔL (mm) is the elongation of film strips at their breaking point and L_0 (mm) is the initial length of the film strips.

2.4.4. Surface morphology. The surface morphology of the films was observed using a scanning electron microscope (JSM-7500 M, JEOL Ltd, Tokyo, Japan). Prior to testing, the films were cut into 5 mm × 5 mm samples, fixed on double-sided adhesive tape, and sputter-plated with gold.[28] Examination was performed at an accelerating voltage of 5 kV and magnification of 200×.

2.4.5. Moisture content (MC). The moisture content (MC) of the composite films was determined using a gravimetric drying method.[29] Square film samples (20 mm × 20 mm) were precisely weighed (M_0) and then dried in an oven at 105 °C for 24 h until a constant weight was achieved. The dried samples were immediately weighed again (M_1) after cooling. Five replicate measurements were performed for each film type, and the MC was calculated using eqn (3).

$$\mathrm{MC}\ (\%) = \frac{M_0 - M_1}{M_0} \times 100 \quad (3)$$

where M_0 is the initial weight of the composite films (g) and M_1 is the final weight of the composite films (g).

2.4.6. Water vapor transmission rate (WVTR). The water vapor transmission rate (WVTR) of the composite films was determined following the method of Yong *et al.* with minor modifications.[30] Anhydrous $CaCl_2$ weighing 3 g was placed in glass test tubes (15 mm inner diameter and 100 mm height), which were then sealed with the films. The initial mass of each assembled tube was recorded. The glass test tubes were subsequently placed in a 6 L chamber containing 300 mL of saturated KCl solution. The tubes were weighed again after 3 days of storage. WVTRs were calculated using eqn (4). Five replicate

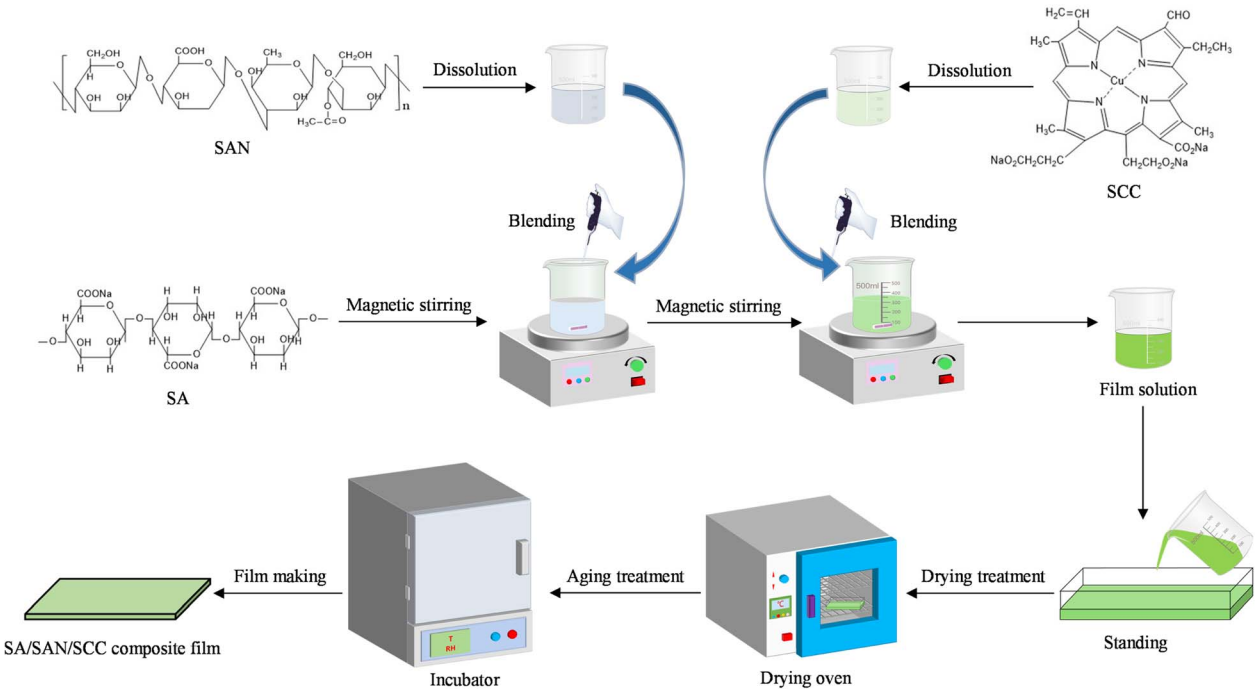

Fig. 1 Preparation of SA/SAN/SCC composite film. SA represents sodium alginate; SAN represents sanxan; SCC represents sodium copper chlorophyllin.

measurements were performed for each film type, and the average WVTR was calculated.

$$\text{WVTR}\ \left(\text{kg d}^{-1}\ \text{m}^{-2}\right) = \frac{M_1 - M_0}{T \times S} \quad (4)$$

where M_0 is the initial weight of the glass test tube (kg), M_1 is the final weight of the test tube (kg), S is the permeation area of the film sample (m^2), and T is the interval time (d).

2.4.7. Carbon dioxide permeability (CDP). Carbon dioxide permeability (CDP) was determined using the method described by Chen *et al.* with slight modifications.[31] KOH weighing 3 g was added to a glass test tube, which was then sealed with a film and weighed. The tubes were then placed in an incubator at constant temperature (25 °C) and humidity (75% relative humidity). The weight of the tubes was determined after 24 h, and difference in the mass of the test tube before and after storage (Δm) was calculated. Five replicate measurements were performed for each film type, and the CDP was calculated using eqn (5).

$$\text{CDP}\ \left(\text{kg d}^{-1}\ \text{m}^{2}\right) = \frac{\Delta m}{A \times D} \quad (5)$$

where Δm is the weight added to the glass test tube (g), A is the area of the film sample (m^2), and D is the test time (d).

2.4.8. Light transmittance and opacity (Op). The transmittance and opacity (Op) of the prepared films (10 mm × 20 mm) were measured in a wavelength range of 200–800 nm at room temperature with a UV–Vis spectrophotometer (L5S, Shanghai Yidian Analytical Instrument Co., Ltd, Shanghai, China).[32] The Op value was calculated using eqn (6).

$$\text{Op} = \frac{A_{600}}{d} \quad (6)$$

where A_{600} is the absorption value at 600 nm and d is the film thickness (mm).

2.4.9. X-ray diffraction (XRD). The X-ray diffraction (XRD) patterns of the films (20 mm × 20 mm) were collected using an X-ray diffractometer (Ultima IV-185, Rigaku Innovative Technologies, Inc.) with Cu-Kα radiation (18 kW) at 40 kV and 40 mA. Scans were performed in a 2θ range of 5°–60° at a scan rate of 5° min^{-1}. Each film had five replicates.

2.4.10. Thermal properties. Thermogravimetric analysis (TGA) and derivative thermogravimetry (DTG) analysis were performed using a thermogravimetric analyzer (TGA/DSC 1/1600HT, Mettler-Toledo Group, Zurich, Switzerland). The test parameters were scanned from room temperature to 600 °C at a heating rate of 10 °C min^{-1} under a constant nitrogen purge.[33] Each film had five replicates.

2.5. Coating and visible light treatments of whole potato

Fresh potato tubers were selected, washed with tap water, and allowed to air-dry under ambient conditions. Subsequently, the tubers were immersed in SA/SAN or SA/SAN/SCC coating solutions for 30 s and removed.[34] The surface solutions were dried. The untreated samples served as the control group (CK). All samples were placed in a ZRG-100B-L cold light source artificial climate incubator (Shanghai Binglin Electronic Technology Co., Ltd, Shanghai, China) and subjected to light treatment at 6000 lux for 12 h at 25 °C and 35% relative humidity. After the light treatment, the samples were transferred to a dark environment at 4 °C for 72 h or 60 days (Fig. 2). The a^* value and total Chl

(TC) content of the whole potato tubers were determined at different storage times to systematically evaluate the effect of composite film coating on the greening of potato tubers.

2.6. Color assessment of whole potato tubers

The a^* values of potato epidermis were measured according to the method described by Wang *et al.* with some modifications.[35] Potato peels with a thickness of 0.2 mm were removed, and the color of the tuber surface was measured using an NR-110 colorimeter (Guangdong San En Shi Intelligent Technology Co., Ltd, Shenzhen, China). Five tubers were taken from each replicate for measurement of a^* values at the stem end, the middle, and the bud end of each tuber immediately before and 48 h or 60 days after visible light treatment. Changes in the overall appearance of whole potato tubers during storage were monitored through photographic imaging.

2.7. Determination of TC content in whole potato tubers

The TC content of the whole potato tubers during storage was measured using the method described by Wassie *et al.* with minor modifications.[36] Potato epidermis weighing 2.0 g was weighed and homogenized with 6 mL of 95% ethanol and then digested for 24 h in the dark. Subsequently, the homogenized samples were centrifuged (TGL-16M, Hunan Xiangyi Laboratory Instrument Development Co., Ltd, China) at 10 280*g* for 10 min at 4 °C. The supernatant was collected and diluted to a final volume of 10 mL with 95% ethanol, and absorbance was measured at 645 and 663 nm using a UV–Vis spectrometer (L5S, Shanghai Edian Analytical Instruments Co., Ltd, Shanghai, China) after thorough mixing. The TC content was calculated using eqn (7).

$$\mathrm{TC}\ (\mathrm{mg/100\ g}) = \frac{(20.21A_{645} + 8.02A_{663}) \times V}{1000 \times m} \times 100 \quad (7)$$

where A_{663} is the absorbance at 663 nm, A_{645} is the absorbance at 645 nm, V is the extraction liquid volume (mL), and m is the sample weight (g).

2.8. Statistical analysis

All experimental treatments were performed with five independent replicates, and each replicate was measured in triplicate. Statistical analyses were performed using IBM SPSS statistics 25.0. All data are presented as mean ± standard deviation, unless otherwise stated. After verifying the assumptions of normality (Shapiro–Wilk test) and homogeneity of variances (Levene's test), inter-group differences were assessed by one-way ANOVA with Dunnett's *post hoc* test. A P-value of less than 0.05 was considered statistically significant. Data visualization and graphical representations were generated using Origin 2022 (OriginLab Corporation, USA).

3. Results and discussion

3.1. Spectral absorption properties of SCC and the effects of environmental factors on its stability

SCC exhibited a characteristic absorption peak at 402 nm (Fig. 3A), indicating strong blue-violet light absorption in the visible spectrum. The material demonstrated notable stability under both light and thermal exposure. After 8 days of light exposure, absorbance decreased by only 6.4%, while samples stored in darkness showed even less reduction (Fig. 3B). Thermal testing revealed excellent stability across a broad temperature range (20–100 °C), with merely a 5.6% decrease in absorbance at 100 °C compared to baseline values at 20 °C (Fig. 3C). SCC also displayed pH-dependent optical properties, achieving optimal performance under alkaline conditions (pH 8–12) while maintaining significant absorbance in weakly acidic environments (pH 4–6) (Fig. 3D). These results collectively demonstrate SCC's exceptional stability and adaptive optical characteristics. Structurally, SCC is a metal–porphyrin derivative synthesized through modification of natural Chl, featuring a copper-coordinated porphyrin ring and three –COONa functional groups attached *via* alkyl chains.[37] The $-COO^-$ groups effectively chelate divalent cations such as Ca^{2+}, inhibiting ion migration, while the porphyrin ring supports the formation of a hydrophobic passivation layer that enhances moisture

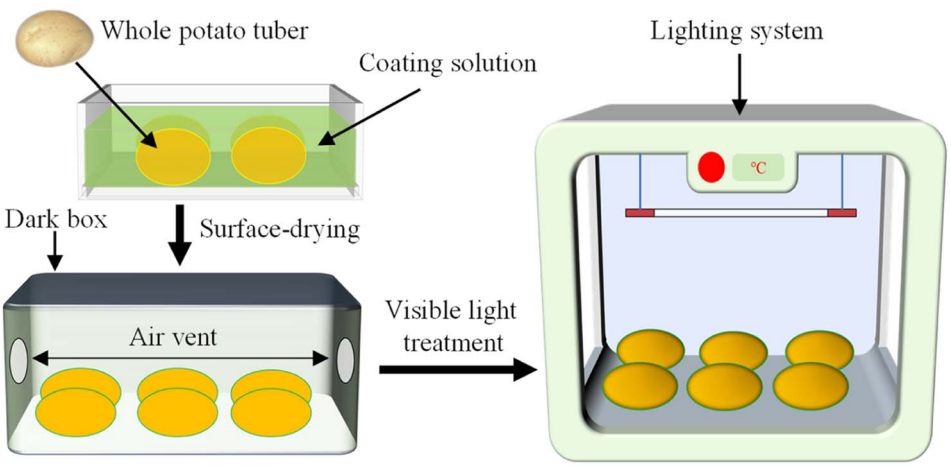

Fig. 2 Coating and visible light treatments of whole potato tuber.

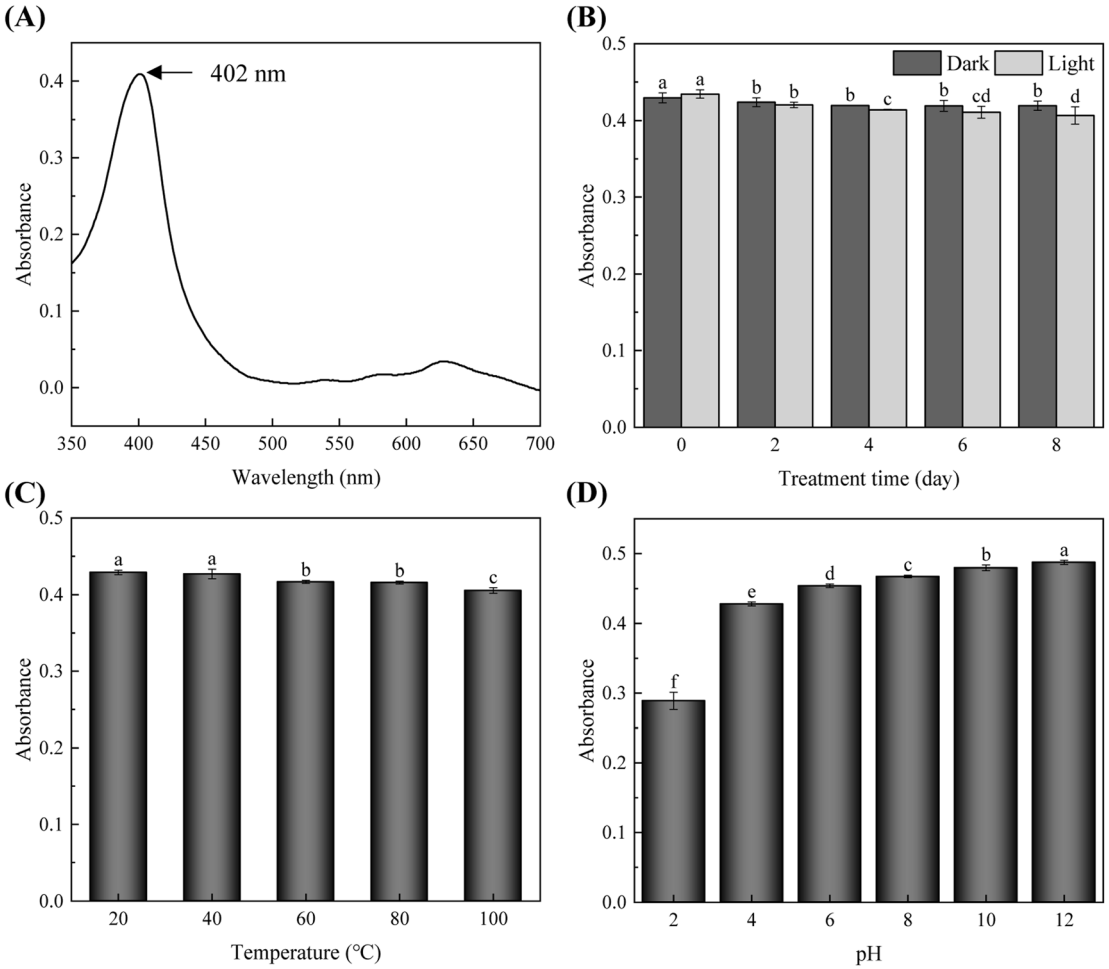

Fig. 3 (A) Spectroscopic absorption characteristics of SCC; effects of (B) illumination duration, (C) temperature, and (D) pH on SCC stability. Values are the means ± standard error ($n = 5$). Different lowercase letters indicate statistically significant differences among treatments ($P < 0.05$).

resistance. These structural attributes contribute to SCC's capacity to improve the thermal stability of composite films.[38] Moreover, blue light can promote Chl synthesis and accumulation in potato tubers, consequently inducing greening.[39] Thus, given the strong absorption of SCC in the blue light spectrum, it can function as an effective light-absorbing material in composite films and can suppress greening in potato tubers.[40]

3.2. Characterization of composite films

3.2.1. Effect of SCC concentration on the visual appearance, thickness, and mechanical properties of SA/SAN/SCC films. Fig. 4A shows a concentration-dependent color gradient in the composite films with SCC incorporation. Control films without SCC were pale-yellow, while increasing SCC concentrations caused a progressive shift toward green tones with greater color depth. The a^* value (CIE lab color space) is used to quantify a color's position on the red-green axis.[41] As shown in Fig. 4B, a^* values decreased significantly ($P < 0.05$) with increasing SCC content, indicating a color shift toward green. The films transitioned from light to deep dark green, consistent with colorimetric data and visual assessments. Li *et al.*[21] demonstrated that SCC strongly absorbs blue-violet light and reflects green light (500–600 nm; Fig. 3A). This behavior explains the chromatic changes: higher SCC loadings intensify blue-violet absorption and enhance green reflection, resulting in a darker green hue.

The thickness of the composite films ranged from 0.0471 mm to 0.0483 mm (Fig. 4C). When the SCC concentration was within 0.4–2.8%, no significant difference in thickness was observed between SA/SAN and SA/SAN/SCC composite films ($P > 0.05$). Nevertheless, at 3.6% SCC concentration, the SA/SAN/SCC composite films exhibited considerably reduced thickness relative to the SA/SAN films ($P < 0.05$). The thickness of the composite film is influenced by multiple factors, primarily including the type of matrix, the proportion of matrix components, the content of biopolymers, and their structural characteristics.[42,43] Thus, excessive SCC concentration may impair its interaction and compatibility with SA/SAN molecules, consequently reducing the thickness of the composite film. However, the SA/SAN/SCC composite films fabricated in this study exhibited thicknesses below 0.3 mm, demonstrating effective barrier properties against environmental factors for food preservation.[17]

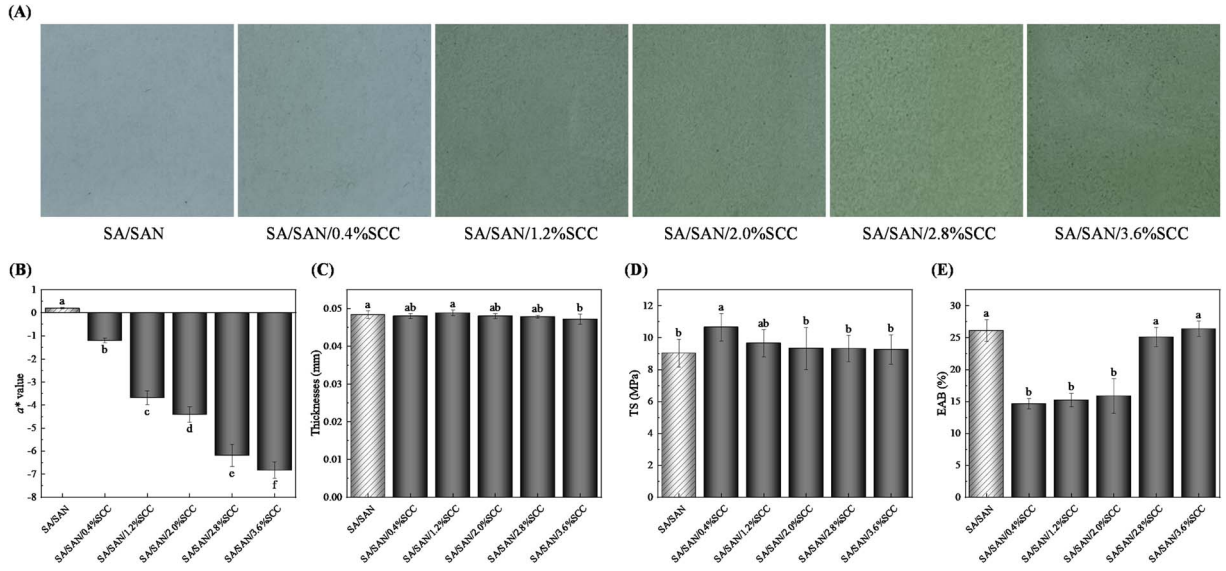

Fig. 4 Visual appearance (A), a^* color values (B), thickness (C), tensile strength (D) and elongation at break (E) of SA/SAN and SA/SAN/SCC composite films. SA/SAN represents the sodium alginate/sanxan crosslinked films, while SA/SAN/SCC indicates films incorporated with sodium copper chlorophyllin. Values are the means ± standard error ($n = 5$). Different lowercase letters indicate statistically significant differences among treatments ($P < 0.05$).

Composite films with high mechanical strength are essential for food packaging applications. TS and EAB are key mechanical indicators.[44] As illustrated in Fig. 4D, the incorporation of 0.4% SCC significantly enhanced the TS of the composite films compared to SA/SAN films ($P < 0.05$), with an 18% increase. However, further increasing the SCC concentration showed no significant improvement in TS ($P > 0.05$). As shown in Fig. 4E, when the SCC addition was in the range of 0.4–2.0%, the EAB of SA/SAN/SCC composite films was significantly lower than that of SA/SAN films ($P < 0.05$). Although the EAB showed an increasing trend with higher SCC content, no significant differences were observed compared to SA/SAN films ($P > 0.05$). Hydrogen bonding between the carboxyl groups of SCC and the hydroxyl groups of SA strengthens the composite film's network structure. This interaction enhances resistance to plastic deformation and significantly improves tensile strength (TS) at optimal SCC concentrations. However, this structural reinforcement also increases brittleness and reduces toughness, resulting in decreased EAB.[45] The mechanical properties of composite films are predominantly governed by molecular interactions within biopolymer matrices.[46] Furthermore, the incorporation of low-concentration SCC may disrupt hydrogen-bonded networks and weaken Ca^{2+}-mediated cross-linking between SA molecules.[47] Collectively, these effects contribute to the reduction in EAB observed in SA/SAN/SCC films.

3.3. Effect of SCC concentration on the surface morphology, MC, WVTR, and CDP of the SA/SAN/SCC films

As shown in Fig. 5A, composite films with 0.4% and 1.2% SCC exhibited relatively smooth and flat surfaces despite some internal bubbles, suggesting good dispersion of SCC within the SA/SAN matrix. However, when the SCC concentration increased to 2–3.6%, the surfaces became noticeably rougher and developed sporadic protrusions, resembling the structure of SA/SAN films. According to Yang *et al.*,[48] adding appropriate amounts of coloring agents such as SCC can modify intermolecular interactions in film-forming matrices (*e.g.*, SA, xanthan gum, or pectin), promoting the formation of homogeneous films with compact and smooth surfaces. Moreover, Wang *et al.*[38] showed that the $-COO^-$ groups in SCC can chelate non-coordinated divalent cations like Ca^{2+}, further enhancing structural compactness. Therefore, by strategically controlling SCC concentration, the microstructure of the composite films can be optimized to improve material performance.

As shown in Fig. 5B, the incorporation of SCC considerably reduced the MC of the composite films compared with the SA/SAN films ($P < 0.05$), although no considerable differences were observed among the SA/SAN/SCC composites ($P > 0.05$). This result suggests that SCC incorporation may reduce the composite film's MC by competitively displacing water molecules from their native binding sites in the polymer matrix. Moreover, owing to the enhanced interaction between SCC and SA/SAN molecules, the spatial structure of the composite film becomes denser,[49] hindering the permeation of water molecules in the environment, restricting the migration of water molecules in the composite film, and further reducing the MC of the composite films.[38]

Composite films with high barrier properties can effectively inhibit the migration of moisture and gases between food and the environment, thereby significantly reducing moisture loss and delaying oxidative deterioration. As shown in Fig. 5C, the incorporation of SCC notably reduced the water vapor transmission rates (WVTRs) of the SA/SAN/SCC films compared to the SA/SAN film. At 2% SCC content, the WVTR was approximately 11% lower than that of the control group ($P < 0.05$),

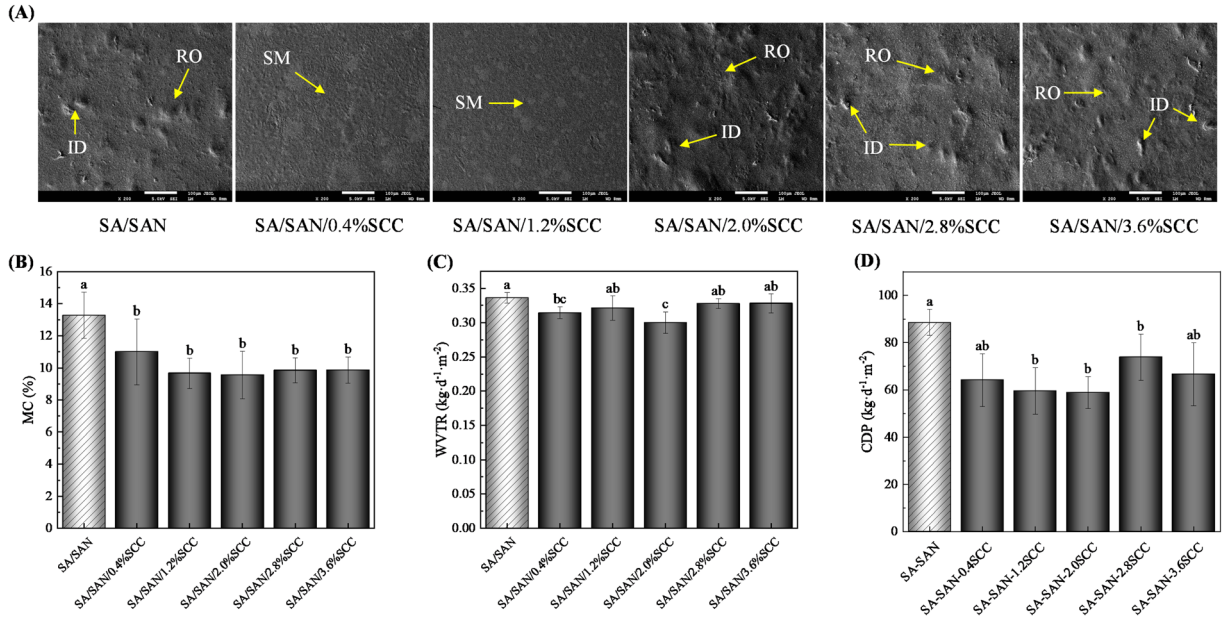

Fig. 5 Microstructural and barrier properties of SA/SAN and SA/SAN/SCC composite films: (A) surface morphology (SEM, 200× magnification), (B) moisture content, (C) water vapor transmission rate (WVTR), and (D) carbon dioxide (CO_2) permeability. SA/SAN represents sodium alginate/sanxan crosslinked films, while SA/SAN/SCC indicates films incorporated with sodium copper chlorophyllin. SM represents smooth; ID represents indentation; RO represents rough. Values are means ± standard error ($n = 5$). Different lowercase letters indicate statistically significant differences among treatments ($P < 0.05$).

indicating that SCC effectively hinders water molecule migration within the film. This reduction in WVTR is closely associated with microstructural changes. The addition of SCC enhances intermolecular interactions between SA and SAN,[48,50] leading to a more compact microstructure that restricts water molecule movement and thereby lowers WVTR.[51] Similarly, as depicted in Fig. 5D, SCC incorporation significantly decreased the carbon dioxide permeability (CDP) of the composite films ($P < 0.05$). The CDP reached its minimum when the SCC content was 1.2% and 2%. This can be attributed to two main factors: firstly, hydrophilic groups in SCC molecules (–COOH, electronegative atoms, and copper ions) can form hydrogen bonds with hydroxyl groups in SA or SAN, creating a dense network that inhibits CO_2 diffusion;[52] secondly, $-COO^-$ groups in SCC can chelate free Ca^{2+} ions, further enhancing the structural compactness of the film and increasing resistance to carbon dioxide permeation.[38]

3.4. Light transmittance, Op, XRD, and thermal properties

The light transmittance and Op value of materials are critical performance indicators for food packaging because these optical properties not only determine the visual appearance of packaging in terms of brightness and darkness but also considerably impact consumer perception and acceptance. Furthermore, these characteristics profoundly influence the visual presentation and sensory evaluation of packaged food products.[38] As shown in Fig. 6A, the SA/SAN/SCC composite films exhibited a concentration-dependent decrease in light transmittance with increasing SCC content, while SA/SAN films remained highly transparent. All SCC-containing films showed strong UV-blocking ability, with less than 20% transmittance in the 200–315 nm range (UVC and UVB). In the visible region (400–450 nm), transmittance was significantly lower than that of SA/SAN films, confirming SCC selective barrier effect against blue light. This is particularly relevant for inhibiting potato greening, as blue light is a major promoter of this process.[6] Therefore, utilizing the UV-blue light blocking properties of SCC can considerably enhance the anti-greening effect of composite films. Fig. 6B shows that at 0.4% and 1.2% SCC, the Op values of the composite films did not differ significantly from those of SA/SAN films ($P > 0.05$). However, higher SCC concentrations led to a marked increase in Op ($P < 0.05$), indicating a substantial impact on optical properties. SCC absorbs strongly in the visible range—especially blue-violet light—reducing transmittance, imparting a dark-green color, and raising Op.[21] Additionally, SCC may disrupt polymer chain alignment, lower crystallinity, and create density variations within the film.[53] These structural changes can lead to micro-scale roughness, enhancing light scattering and further reducing transparency.

The characteristic peaks in XRD can reflect the compatibility and interaction strength between components in composite films.[24] As shown in Fig. 6C, the XRD patterns of the SA/SAN and SA/SAN/SCC composite films exhibited similar trends, and four characteristic diffraction peaks were observed at 9.26°, 21.08°, 23.12°, and 28.98°. As SCC concentration further increased, the three diffraction peaks at 9.26°, 21.08°, and 28.98° in the SA/SAN/SCC composite films became considerably broader and weaker than those in the SA/SAN films. These changes indicate that the incorporation of SCC reconstructed the intermolecular hydrogen bonding network, disrupting the original ordered

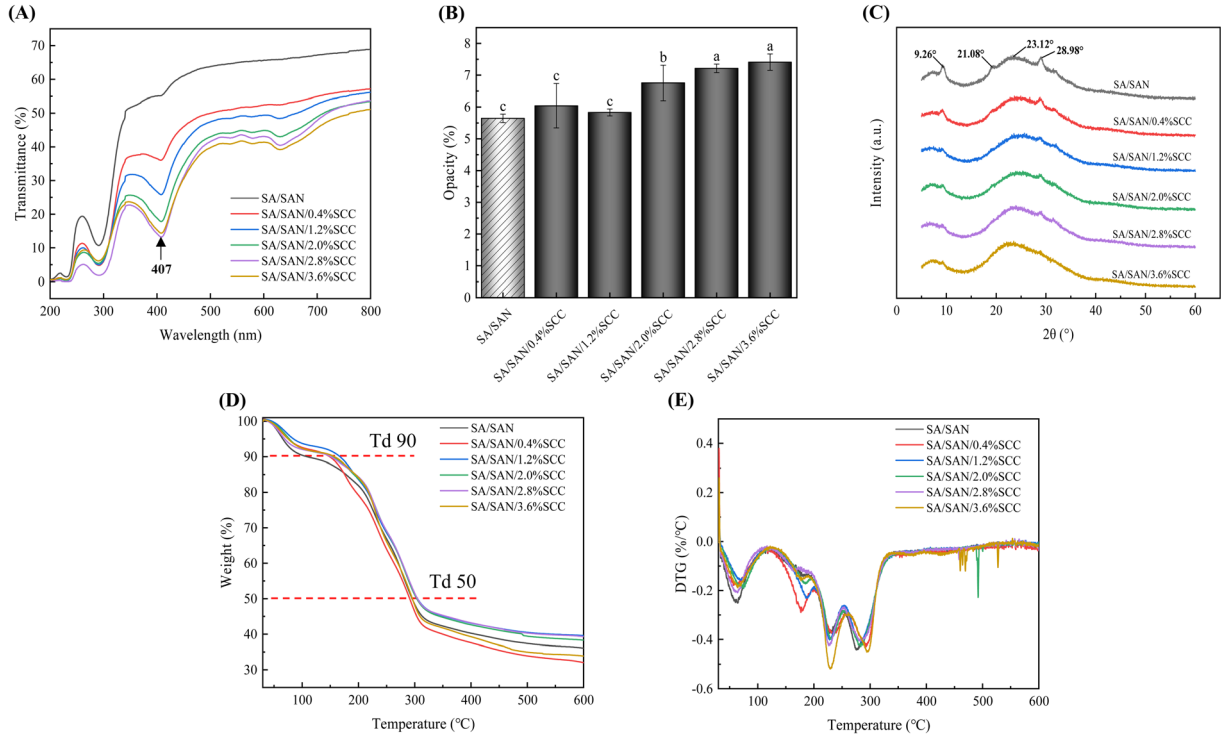

Fig. 6 Transmittance (A), opacity (B), X-ray diffraction pattern (C), and thermal properties (D and E) of SA/SAN and SA/SAN/SCC composite films. SA/SAN represents sodium alginate/sanxan crosslinked films, while SA/SAN/SCC indicates films incorporated with sodium copper chlorophyllin. Values are the means ± standard error ($n = 5$). Different lowercase letters indicate statistically significant differences among treatments ($P < 0.05$).

molecular arrangement of SA/SAN (or increasing the amorphous regions) and thereby reducing the crystallinity of the SA/SAN/SCC composite films.[54] Notably, when the SCC concentration was within the range of 0.4–2.0%, the diffraction intensity of the main peak (23.12°) gradually decreased, confirming good compatibility and strong intermolecular interactions between SCC and SA/SAN molecules.[55] XRD analysis further revealed that an appropriate amount of SCC maintained the original mechanical properties of the SA/SAN composite films (Fig. 4D and E).[56] Thus, the mechanical properties and changes in crystallinity in the SA/SAN/SCC composite films were fundamentally governed by the dynamic balance of intermolecular interactions.

TGA and DTG analysis can reflect the thermal stability of materials.[57] As shown in Fig. 6D, all composite films displayed similar weight loss trends, undergoing three main decomposition stages. The first stage (30–120 °C) involved about 10% weight loss, mainly due to moisture evaporation. The SA/SAN/SCC films showed less weight loss in this stage compared to SA/SAN films. The second stage (130–350 °C) was the major decomposition phase, involving dehydration, depolymerization of polysaccharide rings, and glycerol evaporation.[58,59] The third stage (350–600 °C) showed a slower weight loss, corresponding to the breakdown of carbonaceous residues.[60] According to the results of Td90 (the temperature at 90% residual mass) and Td50 (the temperature at 50% residual mass), the SA/SAN/SCC films had higher Td90 temperatures than SA/SAN films. Those with 1.2–2.8% SCC also exhibited higher Td50 values, indicating better thermal stability. The DTG curves (Fig. 6E) showed that, except for the 2.8% SCC film, SA/SAN/SCC films had higher peak temperatures between 150 and 250 °C, further confirming that suitable SCC content improves thermal stability.

The analyses suggest a correlation between thermal and mechanical properties. At optimal concentrations, SCC enhances intermolecular interactions, improving both thermal and mechanical performance. Excessive or insufficient SCC disrupts these interactions, reducing overall properties. The TGA and DTG variations confirm structural changes in the film network, underscoring the importance of optimizing SCC content to achieve balanced performance.

3.5. Effects of different coating treatments on whole potato greening

After 72 hours of storage, the a^* values decreased across all groups (Fig. 7A), indicating enhanced greening in whole potato tubers. Notably, samples coated with SA/SAN/SCC composites exhibited significantly higher a^* values compared to the control and SA/SAN-treated groups ($P < 0.05$). Within the SCC concentration range of 0.4% to 2.8%, no significant differences in a^* values were observed among the SA/SAN/SCC-treated groups during the three-day storage period ($P > 0.05$). Meanwhile, TC content increased significantly in both the control and all coating groups after 72 hours compared to initial levels (0 day; Fig. 7B). However, TC content in tubers coated with SA/SAN/SCC composites was significantly lower than in the control and SA/

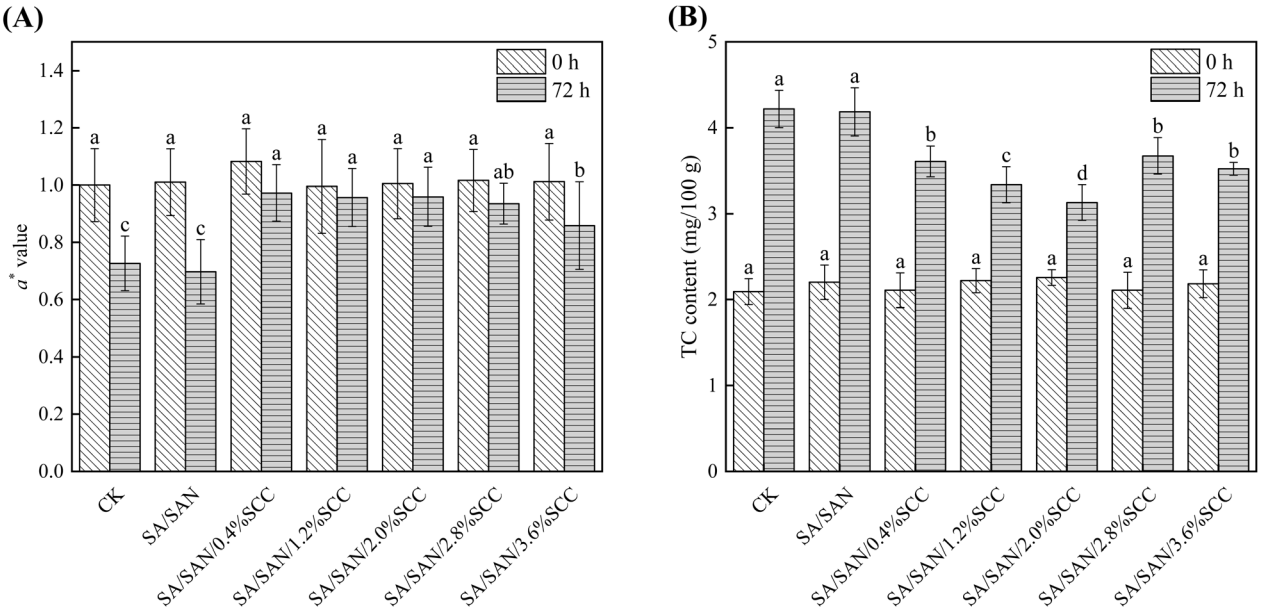

Fig. 7 Effects of SA/SAN and SA/SAN/SCC coating treatments on (A) a^* color values, and (B) total chlorophyll (TC) content in whole potatoes during 3 day storage. CK represents the control group (uncoated samples). SA/SAN represents sodium alginate/sanxan crosslinked films, while SA/SAN/SCC indicates films incorporated with sodium copper chlorophyllin. Values are means ± standard error ($n = 5$). Different lowercase letters indicate statistically significant differences among treatments ($P < 0.05$).

SAN groups ($P < 0.05$). The most effective inhibition was observed at 2% SCC, which resulted in the lowest TC content—25.82% and 25.22% lower than the control and SA/SAN groups, respectively. Moreover, TC content in SA/SAN/SCC-coated samples showed an initial decrease followed by an increase with rising SCC concentration, a trend consistent with that of a^* values. These findings indicate that applying an appropriate concentration (particularly 2%) of SA/SAN/SCC composite coating effectively inhibits Chl biosynthesis and substantially mitigates greening in whole potato tubers.

Potato tubers typically experience a physiological dormancy period of approximately 60 days after harvest, during which metabolic activity remains relatively stable.[61] Changes in overall appearance, a^* value, and TC content in whole potatoes stored at 4 °C for 60 days are shown in Fig. 8. Throughout the storage period, tubers coated with SA/SAN/SCC consistently exhibited better overall appearance (Fig. 8A) and higher a^* values (Fig. 8B) compared to the SA/SAN-coated and control groups. Although no significant difference in a^* values was observed between the SA/SAN/SCC and SA/SAN groups at day 60 ($P > 0.05$), the SA/SAN/SCC treatment resulted in a 15.12% higher a^* value than the SA/SAN group at day 30 ($P < 0.05$). As shown in Fig. 8C, TC content increased significantly over time in all groups ($P < 0.05$). The SA/SAN/SCC coating consistently maintained lower TC levels compared to both the SA/SAN and control groups throughout the 60 day period. After 30 days, the TC content in the SA/SAN/SCC-treated tubers was 18.35% and 24.41% lower than in the SA/SAN and control groups, respectively ($P < 0.05$). These results demonstrate that the SA/SAN/SCC coating effectively inhibited greening over the 60 day storage, with particularly pronounced suppression during the first 30 days.

Light is a major environmental factor that induces Chl synthesis in potato tubers. Upon light exposure, amyloplasts in tubers gradually differentiate into chloroplasts, promoting Chl production in surface cells and ultimately leading to skin greening.[2] Notably, different light spectra vary considerably in their ability to induce Chl accumulation. Dhalsamant *et al.*[5] reported that blue and red light are particularly effective in promoting Chl synthesis. Tanios *et al.*[6] further demonstrated that blue light induces significantly stronger greening than red light. Li *et al.*[21] identified two characteristic absorption peaks of SCC at 405 nm and 630 nm, a finding consistent with the results presented in Fig. 3A. This absorption behavior is attributed to the synergistic interaction between the conjugated porphyrin ring system and Cu^{2+} ions (Witte *et al.*;[62] Zhao *et al.*[37]). The core structure of SCC consists of a highly conjugated porphyrin macrocycle formed by four pyrrole rings. This π-electron system enables selective light absorption at specific wavelengths, inducing $\pi \rightarrow \pi^*$ electronic transitions that produce the characteristic spectrum: the Soret band at 405 nm corresponds to transition to the second excited state, while the Q band at 630 nm arises from transition to the first excited state. The reduction in TC content observed in this study is likely associated with the light-absorbing properties of SCC. Incorporating SCC significantly improved the barrier performance of SA/SAN/SCC composite films against both UV (200–315 nm) and blue light (400–500 nm) (Fig. 6A), thereby reducing light-induced Chl synthesis and resulting in lower TC content in tubers (Fig. 8C).

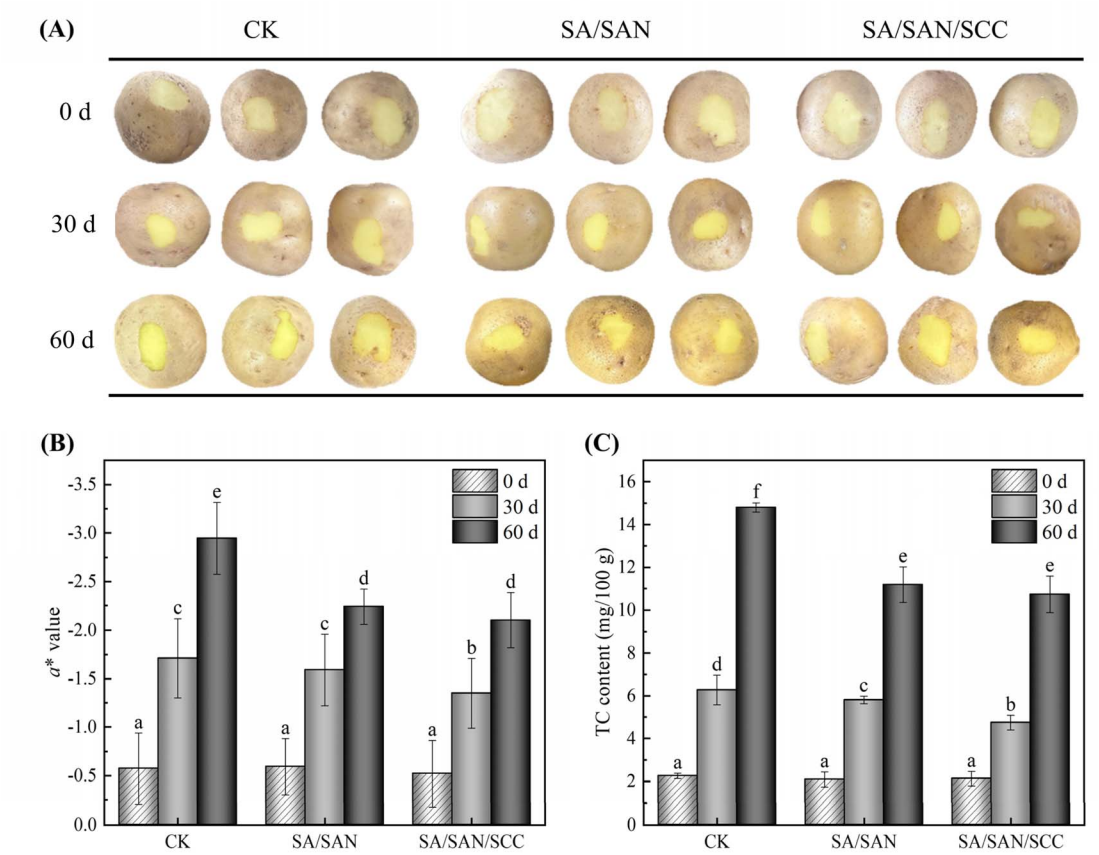

Fig. 8 Effects of SA/SAN and SA/SAN/SCC coating treatments on (A) visual appearance, (B) a^* values, and (C) total chlorophyll (TC) content in whole potatoes during 60 day storage at 4 °C. CK represents the control group (uncoated samples). SA/SAN represents sodium alginate/sanxan crosslinked films, while SA/SAN/SCC indicates films incorporated with sodium copper chlorophyllin. Values are means ± standard error ($n = 5$). Different lowercase letters indicate statistically significant differences among treatments ($P < 0.05$).

3.6. Limitations and practical feasibility for industrial implementation

Although the SA/SAN/SCC composite film shows significant effectiveness at the laboratory scale, its transition to industrial-scale application still faces challenges and requires comprehensive comparison with existing commercial solutions. Compared to opaque plastic packaging, the developed film does not achieve complete light blockage. Instead, it utilizes SCC to enable spectral-selective barrier properties against ultraviolet (200–315 nm) and blue light (400–450 nm). While its efficacy in greening inhibition is slightly inferior to that of completely light-proof opaque packaging, it offers the advantage of good visibility of the packaged potatoes, facilitating quality inspection and consumer selection. Moreover, its bio-based and biodegradable nature provides a distinct advantage in environmental sustainability over conventional plastics. In comparison with conventional ultraviolet (UV)-blocking films, the protective scope of this film extends beyond the UV spectrum. More critically, it effectively blocks blue light, which has been demonstrated to be a major contributor to the induction of potato greening,[6,40] thus representing a more targeted approach for greening suppression. At the industrial level, the core challenge lies in precise process control during production. The primary issue in scaling lies in maintaining optimal SCC dispersion within the SA/SAN matrix at concentrations above 2.8%, as higher loadings induce aggregation that compromises film homogeneity, thickness uniformity, and mechanical properties. Industrial-scale processing necessitates precise control of shear forces, mixing parameters, and solvent evaporation rates to prevent agglomeration and ensure consistent film quality. Furthermore, the pH-responsive behavior of SCC demands strict environmental control to achieve reproducible optical performance across production batches. From an economic perspective, the semi-synthetic production process of SCC increases material costs by approximately 15–20% compared to conventional SA/SAN films. Nevertheless, this cost premium is offset by significant functional benefits, including a 25.82% reduction in potato greening within 72 h and sustained protective efficacy over 60 days, which substantially reduces postharvest losses in high-value crops. Future work will focus on optimizing SCC synthesis and identifying cost-effective biological precursors to improve economic viability. This film offers environmental benefits as a biodegradable, bio-based packaging that reduces food waste's carbon footprint. However, its potential risks, particularly concerning copper ion leaching and SCC ecotoxicity, require thorough investigation. Life-cycle

assessments and toxicological studies are crucial to ensuring its overall safety and environmental advantage.

In conclusion, despite the challenges related to scalability, cost, and environmental verification, SA/SAN/SCC films demonstrate strong potential for industrial adoption. Technical obstacles can be mitigated through process optimization, and the economic model becomes favorable when considering the value of reduced food waste. Although further environmental validation is needed, this technology is particularly suited for high value produce where preservation is economically critical, thereby supporting sustainable postharvest management practices.

4. Conclusions

This study successfully developed an SA/SAN/SCC composite coating film and systematically evaluated its effectiveness in inhibiting potato tuber greening. First, the composite film demonstrated exceptional physical and optical properties, and SCC incorporation effectively blocked UV (200–315 nm) and blue light (400–450 nm) transmission (<20% and <40% respectively). Film thickness was optimally maintained at 0.047–0.048 mm, preserving its protective functionality while minimizing material usage. Second, the mechanical and barrier properties were considerably enhanced. At optimal concentrations (0.4–2.0% SCC), TS increased by 18%, whereas WVTR decreased by 11%. The films showed improved carbon dioxide barrier properties, and the lowest permeability was achieved at 1.2–2.0% SCC concentrations. Notably, the SA/SAN/SCC coating demonstrated remarkable anti-greening effects during potato storage. After 72 h, the 2% SCC formulation reduced Chl content by 25.82% compared with the controls, and sustained inhibition was observed throughout 60 days of long-term storage. Coated potatoes maintained better visual quality (high a^* values) and significantly lower Chl levels than the uncoated controls and SA/SAN-treated samples. These results confirm that SA/SAN/SCC composite coatings inhibit the greening of potato tubers, offering a novel packaging solution for the postharvest preservation of agricultural products. However, assessments of sensory characteristics, consumer acceptance, and shelf-life extension are critical to validating the commercial potential of food packaging technologies. Future studies should prioritize the sensory characteristics, consumer acceptance, and shelf-life extension evaluations, conducted alongside analysis of potato quality at varying storage temperatures, to better predict consumer behavior and practical application value. Furthermore, investigations into the long-term stability and safety of the film remain equally essential.

Author contributions

Erihemu: writing–review & editing, writing–original draft, supervision, project administration, funding acquisition, formal analysis. Chuchu Zhang: writing – review & editing, software, visualization, investigation. Hongze Lv: writing–review & editing, software, investigation. Ke Shi: writing–review & editing, investigation, supervision. Jing Wang: writing–review & editing, investigation, formal analysis. Fan Yang: writing–review & editing, supervision, conceptualization. Yi Wu: visualization, investigation, formal analysis. Hui Ma: visualization, formal analysis. Pengfei Zhang: investigation, formal analysis, conceptualization. Wenliang Qi: formal analysis, visualization, investigation.

Conflicts of interest

The authors declare no competing interests.

Data availability

The datasets obtained during the current study are available from the corresponding author upon reasonable request.

Acknowledgements

This work was financially supported by the National Natural Science Foundation of China (No. 31701667), Shanxi Provincial Department of Education (No. 2024SJ232; 2024JD05), and the Application Foundation Research Program of Shanxi Province (No. 20210302123334).

References

1 L. G. Moens, J. Van Wambeke, E. De Laet, J.-C. Van Ceunebroeck, P. Goos, A. M. Van Loey and M. E. G. Hendrickx, Effect of postharvest storage on potato (Solanum tuberosum L.) texture after pulsed electric field and thermal treatments, *Innovative Food Sci. Emerging Technol.*, 2021, **74**, 102826, DOI: **10.1016/j.ifset.2021.102826**.

2 S. Tanios, T. Thangavel, A. Eyles, R. S. Tegg, D. S. Nichols, R. Corkrey and C. R. Wilson, Suberin deposition in potato periderm: A novel resistance mechanism against tuber greening, *New Phytol.*, 2020, **225**, 1273–1284, DOI: **10.1111/nph.16334**.

3 H. Zhang, X. Liu, H. Nie, B. Song, P. Du, S. Liu, L. Li and Z. Zhao, Nitrogen management can inhibit or induce the sprouting of potato tubers: Consequences of regulation tuberization, *Postharvest Biol. Technol.*, 2022, **183**, 111722, DOI: **10.1016/j.postharvbio.2022.111722**.

4 H. Okamoto, L. J. M. Ducreux, J. W. Allwood, P. E. Hedley, A. Wright, V. Gururajan, M. J. Terry and M. A. Taylor, Light regulation of chlorophyll and glycoalkaloid biosynthesis during tuber greening of potato S. tuberosum, *Front. Plant Sci.*, 2020, **11**, 753, DOI: **10.3389/fpls.2020.00753**.

5 K. Dhalsamant, C. B. Singh and R. Lankapalli, A review on greening and glycoalkaloids in potato tubers: Potential solutions, *J. Agric. Food Chem.*, 2022, **70**, 13819–13831, DOI: **10.1021/jf9b04278**.

6 S. Tanios, A. Eyles, R. Tegg and C. Wilson, Potato tuber greening: A review of predisposing factors, management and future challenges, *Am. J. Potato Res.*, 2018, **95**, 248–257, DOI: **10.1007/s12230-018-09696-2**.

7 R. Gheorghita (Puscaselu), G. Gutt and S. Amariei, The use of edible films based on sodium alginate in meat product

packaging: An eco-friendly alternative to conventional plastic materials, *Coatings*, 2020, **10**, 166, DOI: 10.3390/coatings10020166.

8 K. B. Biji, C. N. Ravishankar, C. O. Mohan and T. K. S. Gopal, Smart packaging systems for food applications: A review, *J. Food Sci. Technol.*, 2015, **52**, 6125–6135, DOI: 10.1007/s13197-014-1449-0.

9 A. R. A. Hammam, Technological, applications, and characteristics of edible films and coatings: A review, *SN Appl. Sci.*, 2019, **1**, 632, DOI: 10.1007/s42452-019-0630-1.

10 V. Glicerina, L. Siroli, E. Betoret, G. Canali, M. D. Rosa, R. Lanciotti and S. Romani, Characterization and evaluation of the influence of an alginate, cocoa and a bilayer alginate-cocoa coating on the quality of fresh-cut oranges during storage, *J. Sci. Food Agric.*, 2022, **102**, 4454–4461, DOI: 10.1002/jsfa.11799.

11 Z. K. Farahani, M. Mousavi, M. S. Ardebili and H. Bakhoda, The influence of sodium alginate and sodium alginate/WPI as coating material on microcapsules of Jujube extract produced by spray dryer, *J. Food Process. Preserv.*, 2022, **46**, e17175, DOI: 10.1111/jfpp.17175.

12 I. Nicolau-Lapeña, I. Aguiló-Aguayo, B. Kramer, M. Abadias, I. Vinas and P. Muranyi, Combination of ferulic acid with Aloe vera gel or alginate coatings for shelf-life prolongation of fresh-cut apples, *Food Packag. Shelf Life*, 2021, **27**, 100620, DOI: 10.1016/j.fpsl.2020.100620.

13 M. Zhang and H. Chen, Development and characterization of starch sodium alginate-montmorillonite biodegradable antibacterial films, *Int. J. Biol. Macromol.*, 2023, **233**, 123462, DOI: 10.1016/j.ijbiomac.2023.123462.

14 A. Ahmad, N. M. Mubarak, F. T. Jannat, T. Ashfaq, C. Santulli, M. Rizwan, A. Najda, M. Bin-Jumah, M. M. Abdel-Daim, S. Hussain and S. Ali, A critical review on the synthesis of natural sodium alginate based composite materials: An innovative biological polymer for biomedical delivery applications, *Processes*, 2021, **9**, 137, DOI: 10.3390/pr9010137.

15 W. Deng, H. Zheng, Z. Zhu, Y. Deng, Y. Shi, D. Wang and Y. Zhong, Effect of surfactant formula on the film forming capacity, wettability, and preservation properties of electrically sprayed sodium alginate coats, *Foods*, 2023, **12**, 2197, DOI: 10.3390/foods12112197.

16 N. A. Lamani and H. S. Ramaswamy, Composite alginate-ginger oil edible coating for fresh-cut pears, *J. Compos. Sci.*, 2023, **7**, 245, DOI: 10.3390/jcs7060245.

17 N. T. C. Duong, A. Uthairatanakij, N. Laohakunjit, P. Jitareerat and N. Kaisangsri, Cross-linked alginate edible coatings incorporated with hexyl acetate: Film characteristics and its application on fresh-cut rose apple, *Food Biosci.*, 2023, **52**, 102410, DOI: 10.1016/j.fbio.2023.102410.

18 H. Lu, X. Li, H. Yang, J. Wu, Y. Zhang and H. Huang, Preparation and properties of riboflavin-loaded xanthan microcapsules, *Food Hydrocolloids*, 2022, **129**, 107641, DOI: 10.1016/j.foodhyd.2022.107641.

19 K. Wang, J. Wang, L. Chen, J. Hou, F. Lu and Y. Liu, Effect of sanxan as novel natural gel modifier on the physicochemical and structural properties of microbial transglutaminase-induced mung bean protein isolate gels, *Food Chem.*, 2024, **449**, 139147, DOI: 10.1016/j.foodchem.2024.139147.

20 M. Roca and A. Pérez-Gálvez, Absolute chlorophyll composition of commercial green food colorants and coloring foodstuff by HPLC-ESI-QTOF-MS/MS: Copper chlorophyllins, *Food Chem.*, 2023, **436**, 137728, DOI: 10.1016/j.foodchem.2023.137728.

21 H. Hosseini, V. P. Noghabi, H. Saberian and S. M. Jafari, The influence of different gums compared with surfactants as encapsulating stabilizers on the thermal, storage, and low-pH stability of chlorophyllin, *Food Chem.: X*, 2023, **20**, 101020, DOI: 10.1016/j.fochx.2023.101020.

22 J. Li, Y. Peng, X. Han, S. Guo, K. Liang and M. Zhang, Nonlinear optical properties of sodium copper chlorophyllin in aqueous solution, *J. Appl. Biomater. Funct. Mater.*, 2017, **15**(S1), 19–24, DOI: 10.5301/jabfm.5000350.

23 D. Yao, Y. Jiang, M. Daroch and J. Tang, Effect of light conditions on phycoerythrin accumulation by thermophilic cyanobacterium Leptothermofonsia sichuanensis and characterization of pigment stability, *Bioresour. Technol.*, 2024, **413**, 131542, DOI: 10.1016/j.biortech.2024.131542.

24 M. Zhong, S. Huang, H. Wang, Y. Huang, J. Xu and L. Zhang, Optimization of ultrasonic-assisted extraction of pigment from Dioscorea cirrhosa by response surface methodology and evaluation of its stability, *RSC Adv.*, 2019, **9**, 1576–1585, DOI: 10.1039/C8RA07516B.

25 Y. Zhang, L. Zhang, J. Hu, Z. Wang, D. Meng, H. Li, Z. Zhou and R. Yang, The structural characterization and color stabilization of the pigment protein-phycoerythrin glycosylated with oligochitosan, *Food Hydrocolloids*, 2023, **136**, 108241, DOI: 10.1016/j.foodhyd.2023.108241.

26 Q. Dong, R. Gao, X. Liu and L. Li, Fabrication of green light activated ethyl cellulose/erythrosine B photobactericidal film and its application in salmon fillets preservation, *Int. J. Biol. Macromol.*, 2025, **308**, 142376, DOI: 10.1016/j.ijbiomac.2025.142376.

27 J. Tang, C. Huang, W. Liu, X. Zeng, J. Zhang, W. Liu, J. Pang and C. Wu, Preparation and characterization of a konjac glucomannan-based bio-nanocomposite film and its application in cherry tomato preservation, *Food Hydrocolloids*, 2025, **159**, 110689, DOI: 10.1016/j.foodhyd.2024.110689.

28 T. Wang, X. Zhai, X. Huang, Z. Li, X. Zhang, X. Zou and J. Shi, Effect of different coating methods on coating quality and mango preservation, *Food Packag. Shelf Life*, 2023, **39**, 101133, DOI: 10.1016/j.fpsl.2023.101133.

29 H. Chen, X. Meng, F. Zhang, J. Chen, X. Ding, T. Jian, Y. Li and H. Lü, Development of chitosan-carboxymethyl cellulose edible films loaded with blackberry anthocyanins and tea polyphenols and their application in beef preservation, *Food Hydrocolloids*, 2025, **164**, 111198, DOI: 10.1016/j.foodhyd.2025.111198.

30 H. Yong, X. Wang, X. Zhang, Y. Liu, Y. Qin and J. Liu, Effects of anthocyanin-rich purple and black eggplant extracts on the physical, antioxidant and pH-sensitive properties of

chitosan film, *Food Hydrocolloids*, 2019, **94**, 93–104, DOI: 10.1016/j.foodhyd.2019.03.012.

31 K. Chen, J. Jiang, R. Tian, Y. Kuang, K. Wu, M. Xiao, Q. Li and F. Jiang, Properties of konjac glucomannan/curdlan-based emulsion films incorporating camellia oil and the preservation effect as coatings on 'Kyoho' grapes, *Int. J. Biol. Macromol.*, 2024, **258**, 128836, DOI: 10.1016/j.ijbiomac.2023.128836.

32 E. Erihemu, H. Lv, C. Zhang, H. Ma, B. Shi, K. Shi, J. Wang, Y. Wu, P. Zhang and H. Zhu, Formulation development and characterization of sodium alginate cross-linked films incorporated with polydopamine as light-blocking materials: Application on greening inhibition of whole potato tuber, *Food Chem.*, 2025, **478**, 143747, DOI: 10.1016/j.foodchem.2025.143747.

33 S. Chen, Q. Zeng, X. Tan, M. Ye, Y. Zhang, L. Zou, X. Chen and K. Hu, Photodynamic antibacterial chitosan/nitrogen-doped carbon dots composite packaging film for food preservation applications, *Carbohydr. Polym.*, 2023, **314**, 120938, DOI: 10.1016/j.carbpol.2023.120938.

34 H. Li, Y. Jiang, J. Yang, R. Pang, Y. Chen, L. Mo, Q. Jiang and Z. Qin, Preparation of curcumin-chitosan composite film with high antioxidant and antibacterial capacity: Improving the solubility of curcumin by encapsulation of biopolymers, *Food Hydrocolloids*, 2023, **145**, 109150, DOI: 10.1016/j.foodhyd.2023.109150.

35 J. Wang, J. Li, W. Chen, Z. Yang, X. Li, L. Wang, Y. Zhang and L. Shi, The changes in chlorophyll, solanine, and phytohormones during light-induced greening in postharvest potatoes, *Postharvest Biol. Technol.*, 2025, **219**, 113291, DOI: 10.1016/j.postharvbio.2024.113291.

36 M. Wassie, W. Zhang, Q. Zhang, K. Ji and L. Chen, Effect of heat stress on growth and physiological traits of alfalfa (Medicago sativa L.) and a comprehensive evaluation for heat tolerance, *Agronomy*, 2019, **9**, 597, DOI: 10.3390/agronomy9100597.

37 Z. Zhao, C. Hurren, M. Zhang, L. Zhou, J. Wu and L. Sun, In situ synthesis of a double-layer chitosan coating on cotton fabric to improve the color fastness of sodium copper chlorophyllin, *Materials*, 2020, **13**, 5365, DOI: 10.3390/ma13235365.

38 Z. Wang, J. Huang, D. Yun, H. Yong and J. Liu, Antioxidant packaging films developed based on chitosan grafted with different catechins: Characterization and application in retarding corn oil oxidation, *Food Hydrocolloids*, 2022, **133**, 107970, DOI: 10.1016/j.foodhyd.2022.107970.

39 Y. Su, J. Tang, Y. Chen, A. Ali, S. Toufouki, X. Wang, J. Zhang and S. Yao, Development and characterization of a bamboo cellulose-based multifunctional composite film by deep eutectic solvent and gelatin, *Ind. Crops Prod.*, 2023, **204**, 117275, DOI: 10.1016/j.indcrop.2023.117275.

40 S. M. Petrovic, S. M. Savic, S. R. Savic, J. B. Zvezdanovic and M.-E. Barbinta-Patrascu, Chlorophyllin sodium copper salt in hydrogel formulations: Spectrophotometric stability studies and in vitro release, *Chem. Pap.*, 2023, **77**, 2635–2645, DOI: 10.1007/s11696-022-02653-8.

41 A. N. Mohammed, O. P. Chauhan and A. D. Semwal, Onion peel steam distillate as a novel anti-browning agent for use in fresh-cut potato cubes, *Potato Res.*, 2024, **68**, 2285–2304, DOI: 10.1007/s11540-024-09801-5.

42 W. Zhou, Y. He, F. Liu, L. Liao, X. Huang, R. Li, Y. Zou, L. Zhou, L. Zou, Y. Liu, R. Ruan and J. Li, Carboxymethyl chitosan-pullulan edible films enriched with galangal essential oil: Characterization and application in mango preservation, *Carbohydr. Polym.*, 2021, **256**, 117579, DOI: 10.1016/j.carbpol.2020.117579.

43 G. D. Báez, E. E. Llopart, R. P. Berino, A. Moro, R. A. Verdini, P. A. Busti and N. J. Delorenzi, Characterisation of beta-lactoglobulin/sodium alginate dry films, *Int. J. Food Sci. Technol.*, 2022, **57**, 242–248, DOI: 10.1111/ijfs.15402.

44 Y. A. Shah, S. Bhatia, A. Al-Harrasi, F. Oz, M. H. Khan, S. Roy, T. Esatbeyoglu and A. Pratap-Singh, Thermal properties of biopolymer films: Insights for sustainable food packaging applications, *Food Eng. Rev.*, 2024, **16**, 497–512, DOI: 10.1007/s12393-024-09380-8.

45 H. Chen, K. Shang, X. Bian, Z. Zhao, Y. Liu, X. Lin, L. Wang, W. Zhang, X. Hu and X. Guo, Enhanced functional pectin films incorporated with olive fruit extracts prepared by deep eutectic solvents, *Food Packag. Shelf Life*, 2024, **46**, 101361, DOI: 10.1016/j.fpsl.2024.101361.

46 C. Wu, J. Tian, S. Li, T. Wu, Y. Hu, S. Chen, T. Sugawara and X. Ye, Structural properties of films and rheology of film-forming solutions of chitosan gallate for food packaging, *Carbohydr. Polym.*, 2016, **146**, 10–19, DOI: 10.1016/j.carbpol.2016.03.027.

47 L. Xu, B. Zhang, Y. Qin, F. Li, S. Yang, P. Lu, L. Wang and J. Fan, Preparation and characterization of antifungal coating films composed of sodium alginate and cyclolipopeptides produced by Bacillus subtilis, *Int. J. Biol. Macromol.*, 2020, **143**, 602–609, DOI: 10.1016/j.ijbiomac.2019.12.051.

48 J. Yang, Y. Fan, J. Cui, L. Yang, H. Su, P. Yang and J. Pan, Colorimetric films based on pectin/sodium alginate/xanthan gum incorporated with raspberry pomace extract for monitoring protein-rich food freshness, *Int. J. Biol. Macromol.*, 2021, **185**, 959–965, DOI: 10.1016/j.ijbiomac.2021.08.142.

49 L. Qiu, M. Zhang, M. Huang, B. Chitrakar and L. Chang, Fabrication of sodium alginate/apricot peel pectin films incorporated with rose anthocyanin-rich extract for monitoring grass carp (Ctenopharyngodon idellus) freshness, *Food Packag. Shelf Life*, 2023, **39**, 101150, DOI: 10.1016/j.fpsl.2023.101150.

50 S. Shi, X. Xu, Y. Ren, H. Zhang, X. Du, H. Li and X. Xia, Beeswax coating improves the hydrophobicity of sodium alginate/anthocyanin/cellulose nanocrystal indicator film, *Food Hydrocolloids*, 2023, **144**, 108930, DOI: 10.1016/j.foodhyd.2023.108930.

51 L. Marangoni Júnior, R. Garcia da Silva, R. Pioli Vieira and R. M. Vercelino Alves, Water vapor sorption and permeability of sustainable alginate/collagen/SiO_2 composite films, *LWT-Food Sci. Technol.*, 2021, **152**, 112261, DOI: 10.1016/j.lwt.2021.112261.

52 L. Miao, W. C. Walton, L. Wang and Y. Wang, Characterization of polylactic acids-polyhydroxybutyrate based packaging film with fennel oil, and its application on oysters, *Food Packag. Shelf Life*, 2019, **22**, 100388, DOI: **10.1016/j.fpsl.2019.100388**.

53 S. Chavoshizadeh, S. Pirsa and F. Mohtarami, Conducting/smart color film based on wheat gluten/chlorophyll/polypyrrole nanocomposite, *Food Packag. Shelf Life*, 2020, **24**, 100501, DOI: **10.1016/j.fpsl.2020.100501**.

54 W. Lu, M. Chen, M. Cheng, X. Yan, R. Zhang, R. Kong, J. Wang and X. Wang, Development of antioxidant and antimicrobial bioactive films based on oregano essential oil/mesoporous nano-silica/sodium alginate, *Food Packag. Shelf Life*, 2021, **29**, 100691, DOI: **10.1016/j.fpsl.2021.100691**.

55 A. Rashid, A. Qayum, S. A. S. Bacha, Q. Liang, Y. Liu, L. Kang, R. Chi, X. Han, J. Ekumah, M. Virk, X. Ren and H. Ma, Preparation and functional characterization of pullulan-sodium alginate composite film enhanced with ultrasound-assisted clove essential oil nanoemulsions for effective preservation of cherries and mushrooms, *Food Chem.*, 2024, **457**, 140048, DOI: **10.1016/j.foodchem.2024.140048**.

56 Y. Wu, Y. Gao and C. Li, Preparation and characterization of smart indicator films based on gellan gum/modified black rice anthocyanin/curcumin for improving the stability of natural anthocyanins, *Int. J. Biol. Macromol.*, 2023, **253**, 127436, DOI: **10.1016/j.ijbiomac.2023.05.001**.

57 S. Roy and J. W. Rhim, Agar-based antioxidant composite films incorporated with melanin nanoparticles, *Food Hydrocolloids*, 2019, **94**, 391–398, DOI: **10.1016/j.foodhyd.2019.05.050**.

58 M. Yang, Y. Xia, Y. Wang, X. Zhao, Z. Xue, F. Quan, C. Geng and Z. Zhao, Preparation and property investigation of crosslinked alginate/silicon dioxide nanocomposite films, *J. Appl. Polym. Sci.*, 2016, **133**, 43845, DOI: **10.1002/app.43845**.

59 P. Kanmani and J. Rhim, Physicochemical properties of gelatin/silver nanoparticle antimicrobial composite films, *Food Chem.*, 2014, **148**, 162–169, DOI: **10.1016/j.foodchem.2014.01.016**.

60 H. Wu, D. Xiao, J. Lu, C. Jiao, S. Li, Y. Lei, D. Liu, J. Wang, Z. Zhang, Y. Liu, G. Shen and S. Li, Effect of high-pressure homogenization on microstructure and properties of pomelo peel flour film-forming dispersions and their resultant films, *Food Hydrocolloids*, 2020, **102**, 105628, DOI: **10.1016/j.foodhyd.2020.105628**.

61 A. M. Rady, D. E. Guyer, I. R. Donis-González, W. Kirk and N. J. Watson, A comparison of different optical instruments and machine learning techniques to identify sprouting activity in potatoes during storage, *J. Food Meas. Charact.*, 2020, **14**, 3565–3579, DOI: **10.1007/s11694-020-00590-2**.

62 K. Witte, I. Mantouvalou, R. Sánchez-de-Armas, H. Lokstein, J. Lebendig-Kuhla, A. Jonas, F. Roth, B. Kanngießer and H. Stiel, On the electronic structure of Cu chlorophyllin and its breakdown products: A carbon K-edge X-ray absorption spectroscopy study, *J. Phys. Chem. B*, 2018, **122**, 1846–1851, DOI: **10.1021/acs.jpcb.7b12108**.